Role of neutrons in the coexistence of magnetic and antimagnetic rotation bands in ^{107}Cd

Deepika Choudhury,[*] R. Palit, P. Singh, J. Sethi, S. Saha, S. Biswas, H. C. Jain, V. Nanal, R. G. Pillay, R. Donthi,
S. K. Jadhav, and B. S. Naidu

Department of Nuclear and Atomic Physics, Tata Institute of Fundamental Research, Mumbai 400085, India

B. Maheshwari and A. K. Jain

Department of Physics, Indian Institute of Technology, Roorkee 247667, India

S. C. Pancholi and R. P. Singh

Inter University Accelerator Centre, Aruna Asaf Ali Marg, New Delhi 110067, India

S. Mukhopadhyay, D. C. Biswas, and L. S. Danu

Nuclear Physics Division, Bhabha Atomic Research Centre, Mumbai 400085, India

S. K. Tandel

UM-DAE Centre for Excellence in Basic Sciences, Mumbai 400098, India

L. Chaturvedi

Department of Pure and Applied Physics, Guru Ghasidas Vishwavidyalaya, Bilaspur 495009, India

K. Rojeeta Devi

Department of Physics and Astrophysics, University of Delhi, Delhi 110007, India

Sukhjeet Singh

Department of Physics, Maharishi Markandeshwar University, Mullana, Ambala 133207, India

Negative parity high-spin states of ^{107}Cd have been investigated using the reaction ^{94}Zr(^{18}O,5n), from the γ-ray coincidence events recorded by the Indian National Gamma Array. A magnetic dipole ($M1$) band structure was established for the first time in this nucleus decaying to the low-spin states via several paths. Lifetimes of five in-band levels in this band have been measured using the Doppler shift attenuation method. The experimentally deduced $B(M1)$ values are found to decrease with increasing spin. The experimental observations, interpreted by the tilted axis cranking calculations, suggest that the $M1$ band is developed from the shears mechanism based on the 5qp configuration $\pi(g_{9/2}^{-2}) \otimes \nu(h_{11/2}g_{7/2}^2)$, which is then crossed by another 5qp configuration $\pi(g_{9/2}^{-2}) \otimes \nu(h_{11/2}^3)$. The semiclassical model of the shears mechanism also reasonably reproduces the decreasing trend of the observed $B(M1)$ values as a function of spin, supporting the above interpretation. The present work highlights the unique coexistence of both magnetic and antimagnetic (observed by us earlier) rotation bands in one nucleus arising from the same proton configuration, but different neutron configurations.

I. INTRODUCTION

Nuclei in the $A \sim 110$ region, being in the vicinity of the $Z = 50$ shell closure, are expected to have a low deformation. The region was the focus of study in recent years for the investigation of interesting rotationlike band structures developed from unusual particle alignments. The low-Ω $h_{11/2}$, $g_{7/2}$, $d_{5/2}$ neutron orbitals and the high-Ω $g_{9/2}$ proton orbitals lying near the Fermi surface, play an active role in deciding the nuclear structure and property at various excitation energies. Specific couplings of the low-Ω neutron particles and high-Ω proton holes give rise to exciting phenomena, like magnetic rotation (MR) and antimagnetic rotation (AMR) [1]. The MR

phenomenon (observation of shears bands) was well explored in various mass regions ($A = 80,110,135,190$) [2,3] and was well understood in terms of shears mechanism proposed by Frauendorf [1,4]. The AMR band can be explained using the twin-shears mechanism and may, therefore, also be termed as a twin-shears band ([5] and references therein).

In the shears mechanism, for the multiquasiparticle configuration, the resultant angular momentum vector of the high-Ω proton holes ($\vec{j}_\pi$) and that of the low-Ω neutron particles ($\vec{j}_\nu$) are like the two blades of a shear which are nearly perpendicular to each other near the bandhead, with the total angular momentum vector ($\vec{I}_{sh} = \vec{j}_\nu + \vec{j}_\pi$) lying in between them. Such a neutron-proton coupling results in a finite perpendicular component of the magnetic dipole moment ($\mu_\perp$). The gradual closing of the two blades towards $\vec{I}_{sh}$ generates a sequence of levels connected by $M1$ transitions

*deepika.chry@gmail.com

with a characteristic decrease in $\mu_\perp$, and hence in the $B(M1)$ values ($B(M1) \propto |\mu_\perp|^2$) as a function of spin, now confirmed in many MR bands [6]. On the other hand, the AMR band arises when at least two proton spin vectors are stretched apart, nearly antialigned, and the resultant neutron spin vector is in between them. The high-spin states are generated by the simultaneous closing of the two blades towards the neutron vector, like two shears operating together (twin-shears mechanism). The developed band is linked by weak $E2$ transitions with their strength decreasing with increase in spin.

Because both MR and AMR arise from high-Ω $g_{9/2}$ holes and low-Ω $h_{11/2}$, $g_{7/2}$, $d_{5/2}$ particles, they can be observed in the same nucleus. The even-even ^{108}Cd isotope has MR bands based on the configurations $[\pi(g_{9/2}^{-3}g_{7/2}) \otimes \nu(h_{11/2}g_{7/2})]$ and $[\pi(g_{9/2}^{-3}g_{7/2}) \otimes \nu(h_{11/2}^{3}g_{7/2})]$ [7,8], along with an AMR band with configuration $[\pi(g_{9/2}^{-2}) \otimes \nu(h_{11/2}^{2}g_{7/2}^{2})]$ [9,10]. It would be interesting to investigate coexisting MR and AMR bands based on the same proton configuration, in one nucleus, and to explore the role of neutron configurations causing the two $g_{9/2}$ proton angular momentum vectors to align or antialign giving rise to the MR or AMR band, respectively.

The odd-N ^{107}Cd nucleus, situated in the transitional region between spherical and deformed nuclei, has proven to be a fertile case for the observation of several exciting nuclear phenomena arising from particle alignment and nuclear rotation competing with each other. A number of experiments to study the low-spin states of ^{107}Cd were carried out in the 1970s and 1980s. An earlier work on the high-spin states was carried out by Jerrestam *et al.* [11] in 1992. We discovered in 2013 the first example of multiple AMR bands in ^{107}Cd, based on the same five-quasiparticle (5qp) configuration $\pi(g_{9/2}^{-2}) \otimes \nu(h_{11/2}g_{7/2}^{2})$, with slightly different neutron alignments [12]. With high-Ω $g_{9/2}$ orbital and low-Ω $h_{11/2}$, $g_{7/2}$ and $d_{5/2}$ orbitals lying near the Fermi surface, the nucleus is also expected to develop MR bands with alternate neutron-proton configurations. This encouraged us to further investigate the level scheme of ^{107}Cd to high-spin states with an aim to search for MR bands in this nucleus and study the role of neutron-proton configurations in the observation of both the MR and AMR bands.

In the present work, we have established new MR band structures in ^{107}Cd: a 5qp band being crossed by another 5qp band arising from shears mechanism along with core rotation. A detailed study of the newly explored MR bands along with the earlier observed AMR band, has revealed that the coexisting MR and AMR bands arise from 5qp configurations with the same proton configuration but slightly different neutron configurations. We present the experimental data and analysis in Sec. II. The results are presented in Sec. III, while discussion and summary are presented in Secs. IV and V, respectively.

II. EXPERIMENTAL DETAILS AND DATA ANALYSIS

The high-spin states in ^{107}Cd were populated and investigated using the heavy-ion fusion evaporation reaction ^{94}Zr(^{18}O,5n)^{107}Cd at a beam energy of 90 MeV. The ^{18}O beam was provided by the TIFR-BARC Pelletron-Linac Facility, Mumbai, located at TIFR, Mumbai. An isotopically enriched

(96% enrichment) self-supporting thin ^{94}Zr target of thickness 0.97 mg/cm^2 was used for the experiment. The emitted γ rays were detected using the Indian National Gamma Array (INGA) spectrometer comprising 20 Compton suppressed HPGe clover detectors arranged in six rings (at $40°$, $65°$, $90°$, $115°$, $140°$, and $157°$) with respect to the beam direction [13]. A digital data acquisition (DDAQ) system based on Pixie-16 modules developed by XIA LLC [13,14] was used for collecting the in-beam data. Two- and higher-fold coincidence events were collected in list mode format.

Lifetimes ($\lesssim 1$ ps) of the high-spin states were measured using the Doppler shift attenuation method (DSAM). The data were available from an earlier experiment carried out with the same experimental facility at TIFR, Mumbai. An isotopically enriched ^{94}Zr (96% enrichment) target of thickness 0.9 mg/cm^2 evaporated on ^{197}Au backing of thickness 10 mg/cm^2 was used. During this experiment, the INGA setup comprised 21 Compton suppressed clover detectors and the ^{18}O beam was delivered at a beam energy of 72 MeV. Standard ^{152}Eu and ^{133}Ba radioactive sources were used to calibrate the γ-ray energy and efficiency of the detectors.

Offline calibration and gain matching was carried out using the DAMM analysis program [15]. Proper Doppler correction was carried out at different angles, for the data obtained from the thin target experiment. The γ-γ coincidence events were then sorted into E_γ-E_γ symmetric and angle-dependent asymmetric matrices using the data sorting routine "Multi pARameter time-stamped based COincidence Search program (MARCOS)" developed at TIFR. The E_γ-E_γ-E_γ cube was also constructed for coincidence analysis using the three- and higher-fold coincidence events. The time window for the coincidences was chosen to be 100 ns. The RADWARE [16] and LINESHAPE [17] analysis programs were used for further data analysis. The level scheme of ^{107}Cd was developed on the basis of the coincidence relations, relative intensities, and multipolarities of the γ-ray transitions.

Multipolarity of the γ transitions were determined using a combination of measurements of Directional Correlation of γ-ray de-exciting Oriented states (DCO ratio method) [18] and linear polarization. The DCO ratios were measured using an asymmetric matrix with the x axis corresponding to the detectors at $157°$ and the y axis corresponding to the $90°$ detectors. The DCO ratio,

$$R_{\text{DCO}} = \frac{I_{157°}^{\gamma_1}\left(\text{Gate}_{90°}^{\gamma_2}\right)}{I_{90°}^{\gamma_1}\left(\text{Gate}_{157°}^{\gamma_2}\right)}, \tag{1}$$

was found to be about 0.5(1.0) and 1.0(2.0) for pure dipole and quadrupole transitions, respectively, with the gate on stretched quadrupole (dipole) transitions. These values were estimated from the transitions of known multipolarity.

The linear polarization of the γ-ray transitions was determined using the integrated polarization directional correlation from the oriented nuclei (IPDCO) method [19]. The four clover detectors placed at $90°$ with respect to the beam direction, were used as Compton polarimeters. The experimental polarization asymmetry, Δ_{IPDCO}, was calculated as

$$\Delta_{\text{IPDCO}} = \frac{aN_\perp - N_\parallel}{aN_\perp + N_\parallel}, \tag{2}$$

where $N_\perp$ ($N_\parallel$) denotes the number of γ-ray counts scattered perpendicular (parallel) to the reaction plane. The scaling factor a is a measure of the perpendicular-to-parallel scattering asymmetry within the crystals of the clover detector, and was determined using the decay data of ^{133}Ba and ^{152}Eu radioactive sources. This parameter was found to be 1.00(1) for the 90° detectors. The linear polarization measurement was carried out using two asymmetric matrices corresponding to the parallel and perpendicular segments of the clover detectors (with respect to the reaction plane) along the x axis and the coincident γ rays from all other detectors along the y axis. The positive value of polarization asymmetry indicates the electric nature of the transition, while the negative value implies magnetic transition.

Furthermore, the $B(M1)$ values of a few high-spin excited states of ^{107}Cd were obtained by measuring the lifetimes of the states using the backed target data. The angle-dependent asymmetric matrices, 140° vs all, 90° vs all, and 40° vs all, were used for this purpose. With gates on the all axis, the 140°, 90°, and 40° spectra were used to fit the Doppler broadened line shapes of the γ-ray energies by using the LINESHAPE analysis code developed by Wells [17]. Incorporating the clover geometry of the detectors, the velocity profiles of the recoiling nuclei were generated for groups of detectors at 140°, 90°, and 40°. This was done by simulating the gradual slowing down of the recoil in the target and the backing using Monte Carlo methods, with a time step of 0.001 ps, for 5000 histories of energy loss at different depths. The energy loss was calculated using the electronic stopping powers of Northcliffe and Shilling [20], corrected for shell effects.

For the lineshape analysis, the gating transitions were chosen to be those below the transitions of interest. The energies of the γ-ray transitions and the intensities of the side-feedings into the state were used as input parameters for the lineshape analysis. For a cascade of transitions, assuming 100% side-feeding into the top of the cascade, an effective lifetime of the topmost state was estimated. This effective lifetime was then used as the input parameter to extract the absolute values of the lifetimes of the lower states in the cascade. The side-feeding intensities were determined from the intensity of the gamma rays feeding and depopulating each state and were fixed so as to reproduce the observed intensity pattern of the band. The side-feeding into each state was assumed as a rotational cascade of five transitions. For individual transition energies, the lineshape simulation was carried out varying the background parameters, intensities of the contaminant peaks, and side-feeding quadrupole moments. For each set of parameters, the simulated lineshapes were fitted to the experimental spectra using the χ^2 minimization routines of MINUIT [21]. After minimizing the χ^2 values for each state individually, a global fit of the full cascade, was performed to deduce the lifetimes of all the states in the cascade. The entire procedure of lineshape fitting until the global fit of the full cascade was repeated for the forward and backward spectra. The uncertainty in the lifetimes of the states was determined from the behavior of χ^2 fit in the vicinity of the minimum, using the MINOS routine [21].

III. RESULTS

In this work, we have established a new negative parity magnetic dipole ($M1$) band structure which feeds the low-spin states via several different paths, as shown in Fig. 1. The band structure and the connecting paths, together comprise 33 transitions. Out of these, 10 transitions were reported in an earlier work by Jerrestam *et al.* [11], but could not be connected to the main level scheme. The 520-keV transition, depopulating the 2679-keV state, was earlier reported by Hagemann *et al.* [22]. The remaining 22 transitions have been newly observed in the present work. The earlier reported 10 transitions have also been rearranged and placed in the level scheme. All the transitions have been placed in the level scheme on the basis of their coincidence relations and relative intensities. Double-gated coincidence spectra, obtained from the thin target data, are displayed in Fig. 2, where the in-band
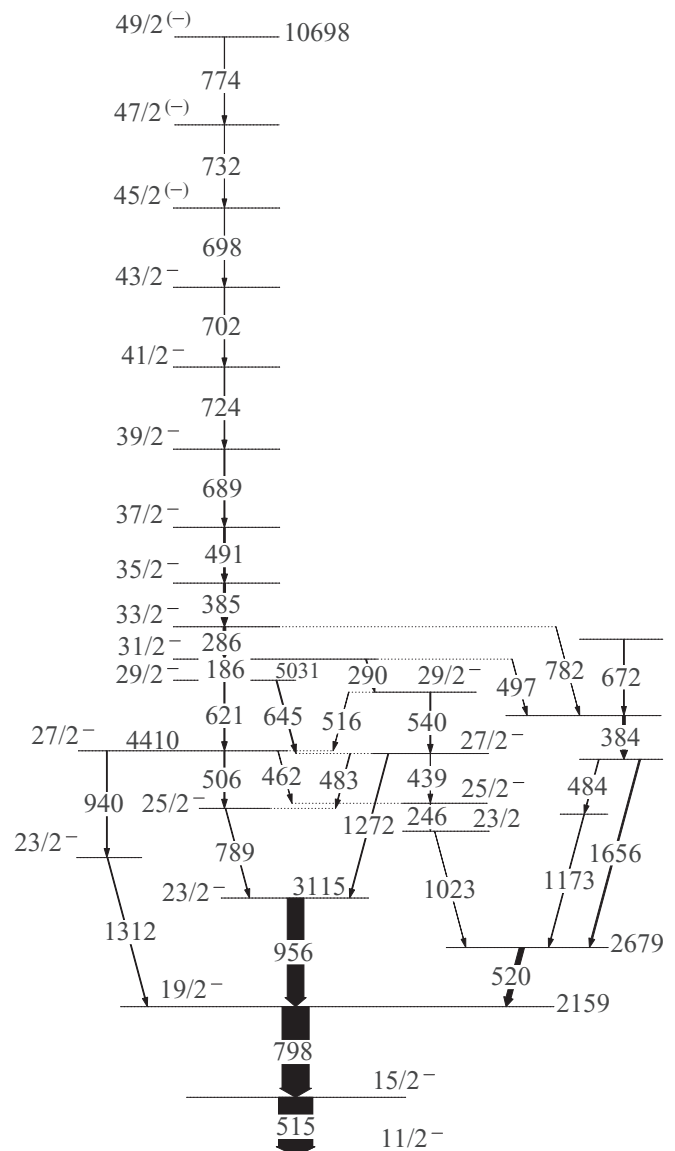
FIG. 1. Partial level scheme of ^{107}Cd.
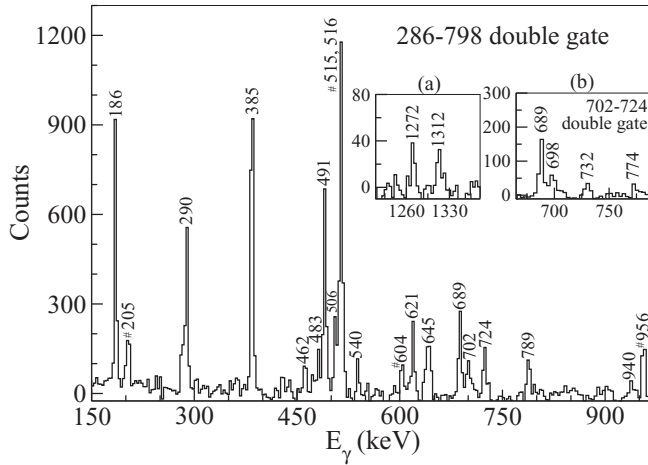
FIG. 2. Double-gated γ-ray coincidence spectrum showing the in-band transitions of the magnetic dipole band along with most of the connecting transitions (connecting the $M1$ band to the low-spin 2159- and 3115-keV states). The spectrum was created with double gate on the 286- and 798-keV transitions. The peaks marked with hash symbols denote the known transitions depopulating the low-spin states [11]. The inset (a) shows the two high energy 1272- and 1312-keV transitions. The inset (b) shows the topmost transitions of the MR band with double gate on the 702- and 724-keV in-band transitions.

transitions of the $M1$ band can be identified along with most of the transitions connecting the band to the 2159- and 3115-keV states.

The spins and parities have been assigned to the states on the basis of the R_{DCO} and Δ_{IPDCO} values of the γ-ray transitions. Figure 3 shows the R_{DCO} values of the transitions obtained with gates on dipole and quadrupole transitions. The Δ_{IPDCO}
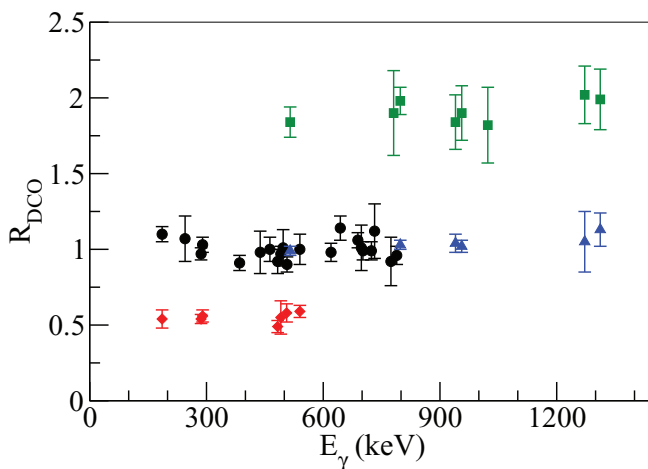
FIG. 3. (Color online) R_{DCO} values for the transitions with gates on dipole and quadrupole transitions. With the gate on dipole transitions, the R_{DCO} values of the dipole and quadrupole transitions are shown by black circles and green squares, respectively. With the gate on quadrupole transitions, the R_{DCO} values of the dipole and quadrupole transitions are shown by red diamond and blue triangular shapes, respectively.
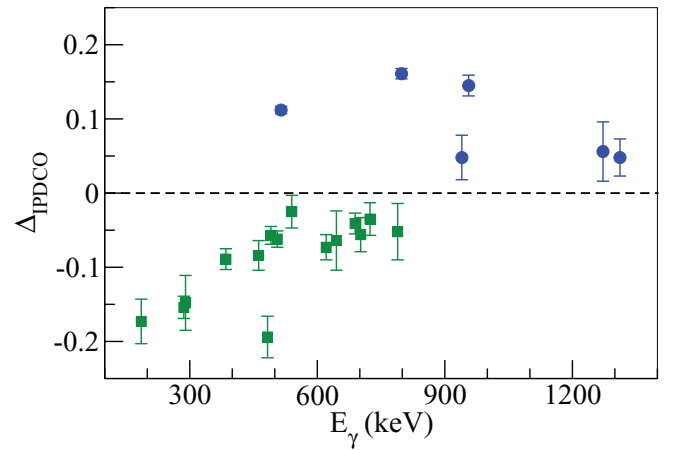
FIG. 4. (Color online) Experimental polarization asymmetry Δ_{IPDCO} values for the transitions. The electric (positive Δ_{IPDCO}) and magnetic (negative Δ_{IPDCO}) transitions are shown by blue circles and green squares, respectively.

values obtained with various possible gates are shown in Fig. 4. The energies, relative intensities, R_{DCO} ratios, polarization asymmetry values, and the adopted multipolarities of the transitions along with the energies and spin-parity assignments of the excited states are listed in Table I.

The $M1$ band structure consists of 10 transitions of energies 186, 286, 385, 491, 689, 724, 702, 698, 732, and 774 keV, establishing the band up to spin $49/2^{(-)}$. A sequence of three transitions of energies 506, 621, and 789 keV, connecting the band to the 3115-keV $(23/2^-)$ state, were found to have $M1$ nature establishing negative parity to the dipole band with a bandhead spin of $29/2^-$. The R_{DCO} ratios and Δ_{IPDCO} values of the 940- and 1312-keV transitions depopulating the 4410- and 3470-keV states, respectively, were found to be consistent with stretched $E2$ character, which further supports the negative parity assignment to the band. The excitation energy, $E_x = 5031$ keV and $I^{\pi} = 29/2^-$ of the bandhead of the $M1$ band structure was further reconfirmed on the basis of the energies and multipolarities of the other γ-ray transitions forming the various paths connecting the band structure to the low-spin 3115- and 2159-keV states.

The 2679-keV state, depopulated by the 520-keV γ-ray transition, is an isomeric state. In an earlier work by Hagemann *et al.* [22], the state was assigned a spin and parity of $21/2^+$. The lifetime of the isomeric state was measured to be 55(4) ns [22]. No spin parity could be assigned to this state from the present work. In addition, no spin and parity could be assigned to the states at excitation energies 3552, 4336, 4720, and 5392 keV, depopulated by the transitions with energies 1173, 484 and 1656, 384 and 672 keV, respectively, because of the presence of the isomer.

The in-band transitions of the $M1$ band structure have been placed on the basis of their coincidence relations and relative intensities. The R_{DCO} and Δ_{IPDCO} values of the transitions up to spin $43/2^-$ confirm their $M1$ nature. The R_{DCO} values of the top three transitions of energies 698, 732, and 774 keV, were observed to be consistent with $\Delta I = 1$ character, but, no polarization measurement could be carried out for these

TABLE I. Energies, relative intensities, DCO ratios for the transitions depopulating the negative parity states of ^{107}Cd. (D) and (Q) represent the R_{DCO} values calculated using gates on dipole and quadrupole transitions, respectively.

E_i (keV)	E_γ(keV)[a]	I_γ	R_{DCO}	Δ_{IPDCO}	Multipolarity	$I_i^\pi \to I_f^\pi$
1360.4	514.8		1.84(10)(D)	0.112(7)	$E2$	$15/2^- \to 11/2^-$
			0.99(3)(Q)			
2158.8	798.4	100	1.98(9)(D)	0.161(9)	$E2$	$19/2^- \to 15/2^-$
			1.03(3)(Q)			
2679.1	520.3	18.9(10)				$\to 19/2^-$
3115.0	956.2	61.5(19)	1.90(18)(D)	0.145(14)	$E2$	$23/2^- \to 19/2^-$
			1.02(4)(Q)			
3470.4	1311.6	3.0(4)	1.99(20)(D)	0.048(25)	$E2$	$23/2^- \to 19/2^-$
			0.96(11)(Q)			
3702.3	1023.2	0.7(2)				$23/2 \to$
3851.9	1172.8	1.9(3)				
3903.8	788.8	2.5(2)	0.96(6)(D)	$-0.052(38)$	$M1$	$25/2^- \to 23/2^-$
3947.8	245.5	1.0(2)	1.07(15)(D)			$25/2 \to 23/2$
4335.5	483.6	2.2(5)				
4335.5	1656.4	5.2(4)				
4386.5	438.7	0.9(1)	0.98(14)(D)			$27/2^- \to 25/2^-$
4386.5	482.7	2.4(2)	0.92(8)(D)	$-0.194(28)$	$M1$	$27/2^- \to 25/2^-$
			0.49(4)(Q)			
4386.5	1271.5	3.1(4)	2.02(19)(D)	0.056(40)	$E2$	$27/2^- \to 23/2^-$
			1.05(20)(Q)			
4410.2	462.4	1.8(2)	1.00(8)(D)	$-0.084(20)$	$M1$	$27/2^- \to 25/2^-$
4410.2	506.4	4.0(4)	0.90(5)(D)	$-0.062(11)$	$M1$	$27/2^- \to 25/2^-$
			0.58(6)(Q)			
4410.2	939.8	3.0(4)	1.84(18)(D)	0.048(30)	$E2$	$27/2^- \to 23/2^-$
			1.04(6)(Q)			
4719.9	384.4[b]					
4926.1	515.9[b]					$29/2^- \to 27/2^-$
4926.1	539.6	3.5(4)	1.00(10)(D)	$-0.035(22)$	$M1$	$29/2^- \to 27/2^-$
			0.59(4)(Q)			
5031.0	620.8	4.0(4)	0.98(6)(D)	$-0.073(17)$	$M1$	$29/2^- \to 27/2^-$
5031.0	644.6	3.5(4)	1.14(8)(D)	$-0.064(40)$	$M1$	$29/2^- \to 27/2^-$
5216.5	185.5	5.5(4)	1.10(5)(D)	$-0.173(30)$	$M1$	$31/2^- \to 29/2^-$
			0.54(3)(D)			
5216.5	290.4	3.3(2)	1.03(5)(D)	$-0.148(37)$	$M1$	$31/2^- \to 29/2^-$
			0.56(4)(Q)			
5216.5	496.6	1.0(2)	1.01(12)(D)			$31/2^- \to$
5391.5	671.6	3.0(5)				
5502.2	285.7	9.7(5)	0.97(4)(D)	$-0.154(15)$	$M1$	$33/2^- \to 31/2^-$
			0.54(3)(Q)			
5502.2	782.3	0.5(1)	1.90(28)(D)			$33/2^- \to$
5886.8	384.6	7.8(5)	0.91(5)(D)	$-0.089(14)$	$M1$	$35/2^- \to 33/2^-$
6377.6	490.8	6.0(4)	0.97(5)(D)	$-0.057(12)$	$M1$	$37/2^- \to 35/2^-$
			0.55(11)(Q)			
7066.4	688.8	3.6(2)	1.06(5)(D)	$-0.041(14)$	$M1$	$39/2^- \to 37/2^-$
7790.7	724.3	2.4(2)	0.99(6)(D)	$-0.045(22)$	$M1$	$41/2^- \to 39/2^-$
8493.1	702.4	1.7(2)	0.99(6)(D)	$-0.056(23)$	$M1$	$43/2^- \to 41/2^-$
9191.6	698.5	1.0(2)	1.01(15)(D)			$45/2^{(-)} \to 43/2^-$
9924.0	732.4	0.6(1)	1.12(18)(D)			$47/2^{(-)} \to 45/2^{(-)}$
10698.3	774.3	0.5(1)	0.92(16)(D)			$49/2^{(-)} \to 47/2^{(-)}$

[a]The uncertainties in the E_γ values lie between 0.5 and 1.0 keV, depending on the intensities.

[b]Intensity, DCO ratio, and polarization measurements were not possible because of the presence of γ rays of overlapping energies.

transitions. Negative parity was assumed for the top three states of the band, as they form a regular band structure.

We measured the lifetimes ($\lesssim 1$ ps) of the states from spin $33/2^-$ to $41/2^-$ in the $M1$ band by the lineshape fitting of the Doppler broadened peaks of the γ-ray transitions depopulating these states. Figure 5 shows the lineshape fits for the transition energies of 286, 385, and 491 keV, depopulating the $33/2^-$-, $35/2^-$-, and $37/2^-$-keV states, respectively, for the
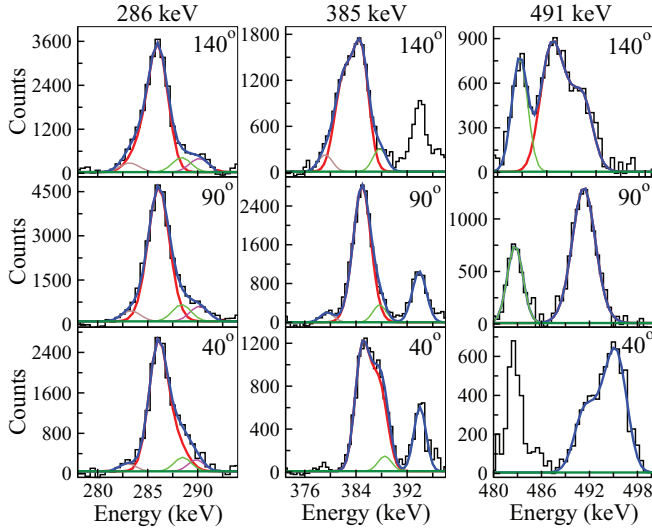
FIG. 5. (Color online) Representative spectra and lineshape fits for the 286-, 385-, and 491-keV transition energies in the $M1$ band of ^{107}Cd for γ-ray spectra at 140°, 90°, and 40° with respect to the beam direction.

gated spectra at angles 140°, 90°, and 40° with respect to the beam direction. The spectra were generated using a sum gate of 186- and 290-keV transitions. The $B(M1)$ values were extracted from the measured lifetimes under the assumption that the observed transitions are pure $M1$ transitions. The deduced lifetimes (τ) and the $B(M1)$ values along with their respective fitting errors are shown in Table II. The obtained $B(M1)$ values of the states decrease with increase in spin from $I^{\pi} = 33/2^{-}$ to $39/2^{-}$, a characteristic feature of an MR band.

IV. DISCUSSION

The newly observed $M1$ band is a prominent feature of the ^{107}Cd nucleus. Interestingly, the band is also observed to have a backbend at $\hbar\omega = 0.72$ MeV. The band was interpreted to be arising from the coupling of two proton holes in the high-Ω $g_{9/2}$ orbitals with three neutron particles in the low-Ω $h_{11/2}$ and $g_{7/2}$ orbitals along with some contribution from the weakly deformed core.

TABLE II. Results of the lineshape analysis for the in-band transitions of the $M1$ band in ^{107}Cd. τ represents the mean lifetime of the state (I_i^{π}) depopulated by γ-ray transition of energy E_{γ}.

$I_i^{\pi} \rightarrow I_f^{\pi}$ ($\hbar$)	E_{γ}(keV)	τ(ps)	$B(M1)(\mu_N)^2$
$33/2^{-} \rightarrow 31/2^{-}$	286	0.671(91)	3.624(491)
$35/2^{-} \rightarrow 33/2^{-}$	385	0.378(44)	2.638(307)
$37/2^{-} \rightarrow 35/2^{-}$	491	0.231(27)	2.084(244)
$39/2^{-} \rightarrow 37/2^{-}$	689	0.194(29)	0.898(134)
$41/2^{-} \rightarrow 39/2^{-}$	724	0.135(20)[a]	1.112(164)[a]

[a]Effective value.

The experimental observations have been interpreted using detailed calculations based on the hybrid version of the tilted axis cranking (TAC) model [23,24]. The model combines the best of the single-particle Woods-Saxon potentials and the modified oscillator potentials (Nilsson model). The single-particle energies of the spherical Woods-Saxon potential are combined with the deformed part of the anisotropic oscillator. The approximation enables the use of a realistic flat bottom potential along with the coupling between the oscillator shells taken into account in a simple way [25]. The values of the neutron and proton pairing gap parameters used for the calculation are $\Delta_n = 1.106$ MeV and $\Delta_p = 0.898$ MeV, respectively, i.e., 80% of the odd-even mass difference. The calculations have been carried out incorporating an attenuation factor of $\eta = 0.8$. The shape parameters follow the Lund convention (ϵ_2, γ) [26].

The magnetic dipole band of ^{107}Cd was assigned five-quasiparticle configuration $\pi(g_{9/2}^{-2}) \otimes \nu(h_{11/2}g_{7/2}^{2})$ (5qp-1). A similar band, based on the same 5qp-1 configuration, was observed in the neighboring odd-A ^{109}Cd isotope (band 10 in Ref. [27]). The band was observed up to spin (39/2^{-}). Figure 6 shows the observed excitation energy [$E(I) - E(I_b)$] (see figure caption) as a function of angular momentum I, and I as a function of rotational frequency $\hbar\omega$ (inset), for the observed MR bands in ^{107,109}Cd. The experimental $\hbar\omega$ ($= dE/dI$) for the dipole transitions was calculated as $\hbar\omega = E_{\gamma}$ (MeV). For ^{107}Cd, the TAC calculations for the 5qp-1 configuration give a minimum in the total energy at a deformation of $\epsilon_2 = -0.118$, $\epsilon_4 = -0.007$, and $\gamma = 48°$ with an average tilt angle $\theta \sim 50°$. The calculated E (MeV) vs I ($\hbar$) and I ($\hbar$) vs $\hbar\omega$ (MeV) values for the 5qp-1 configuration reasonably reproduce the corresponding measured values, as shown in Fig. 7. As shown in Fig. 8, the calculated $B(M1)$ values for the 5qp-1 configuration decrease with increase in
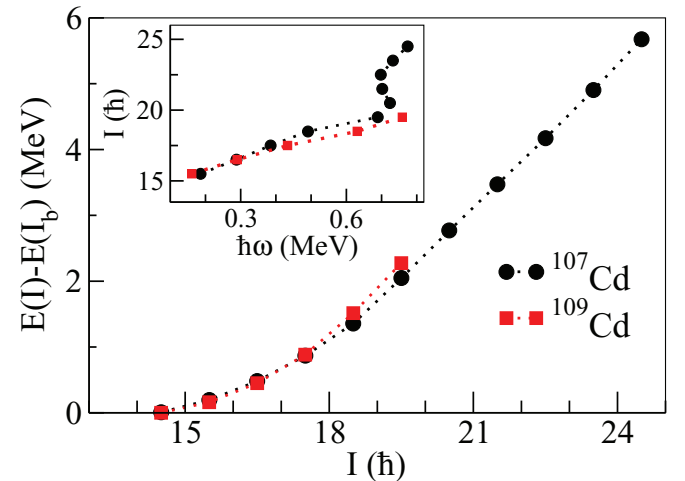
FIG. 6. (Color online) Plot of the observed excitation energy $E(I) - E(I_b)$ as a function of angular momentum I, and I as a function of rotational frequency $\hbar\omega$ (inset), for the MR bands in ^{107,109}Cd. $E(I_b)$ correspond to the excitation energy of the bandhead with spin $29/2^{-}$, which is 5031 keV for the MR band in ^{107}Cd and 4812 keV [27] for the MR band in ^{109}Cd.
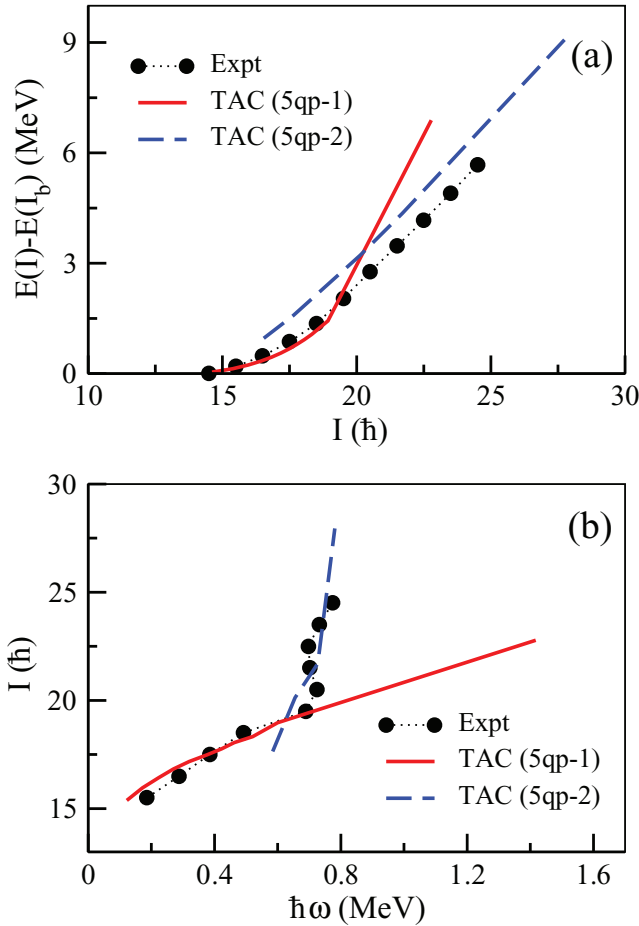
FIG. 7. (Color online) Comparison of the calculated E (MeV) vs I ($\hbar$) values (a) and $I(\hbar)$ vs $\hbar\omega$ (MeV) values (b) with the corresponding measured values, for the negative parity magnetic dipole band in ^{107}Cd. TAC(5qp-1) and TAC(5qp-2) denote the results of TAC calculations using the five-quasiparticle configurations $\pi(g_{9/2}^{-2}) \otimes \nu(h_{11/2}g_{7/2}^2)$ and $\pi(g_{9/2}^{-2}) \otimes \nu(h_{11/2}^3)$, respectively. $E(I_b)$ is the excitation energy of the observed bandhead at spin $29/2^-$.

FIG. 8. (Color online) Comparison of the calculated $I(\hbar)$ vs $B(M1)$ $[(\mu_N)^2]$ values with the corresponding measured values for the MR bands in ^{107}Cd. TAC(5qp-1) and TAC(5qp-2) denote the results of TAC calculations using the five-quasiparticle configurations $\pi(g_{9/2}^{-2}) \otimes \nu(h_{11/2}g_{7/2}^2)$ and $\pi(g_{9/2}^{-2}) \otimes \nu(h_{11/2}^3)$, respectively. For differences in the calculated values of $B(M1)$ for 5qp-1 and 5qp-2, see text.

spin which agrees with the corresponding measured values, a signature of magnetic rotation band.

The backbend observed in the MR band ^{107}Cd is interpreted as from a band-crossing of the 5qp-1 configuration by another 5qp configuration $\pi(g_{9/2}^{-2}) \otimes \nu(h_{11/2}^3)$ (5qp-2). The observed properties of the top part of the band after the backbend have been interpreted on the basis of the TAC calculations for the 5qp-2 configuration. The calculations give a minimum in the total energy at a deformation of $\epsilon_2 = 0.140$, $\epsilon_4 = -0.007$, and $\gamma = 0°$ with an average tilt angle $\theta \sim 70°$. The TAC calculations for the 5qp-1 and 5qp-2 configurations show a band-crossing near spin $20\hbar$ (see Fig. 7). For the 5qp-2 configuration, the TAC calculation gives much lower $B(M1)$ values as compared to those calculated for the 5qp-1 configuration shown in Fig. 8. The calculated $B(M1)$ values, although small, decrease with increase in spin (see Fig. 8), suggesting the generation of high spins from the shears mechanism.

The calculations suggest that the band after the band-crossing, assigned the 5qp-2 configuration, has slightly larger deformation which is nearly prolate in nature. Its calculated $B(M1)$ values are around $0.5(\mu_N)^2$ and the $B(E2)$ values around $0.1 \sim (eb)^2$. In comparison, the lower part of the band, assigned the 5qp-1 configuration, has $B(M1) \sim 2(\mu_N)^2$ and $B(E2) \sim 0.01(eb)^2$ near the band-crossing. The 5qp-2 band has a larger $B(E2)$, but is still typical of the values seen in MR bands. Moreover, the calculated $B(E2)$s remain nearly constant with increasing spin in the 5qp-2 band. This suggests that the rotational contribution remains constant in the upper band. We, therefore, interpret the 5qp-2 band as a weak MR band with a constant rotational contribution. Because the crossover $E2$ transitions will be very weak and have a high energy (about 1.4 MeV), they remain unobserved.

The calculations, therefore, successfully explain the observed properties of the band structure on the basis of shears mechanism along with the core contribution. The resultant of two high-Ω $g_{9/2}^{-2}$ proton angular momentum vectors $\vec{j}_\pi$, and the resultant of the low-Ω $h_{11/2}$ and $g_{7/2}^2$ neutron angular momentum vectors $\vec{j}_\nu$, when nearly perpendicular to each other, form the bandhead of the shears band. The high-spin states arise from the gradual closing of the neutron-proton vectors up to spin $39/2^-$. At this excitation energy, the neutron-proton blades reopen because all three neutron particles are now occupying only the $h_{11/2}$ orbitals. The band structure further extends to high-spin states because of the closing of these blades along with the contribution from the core rotation.

The decreasing trend of the observed $B(M1)$ values (before the backbending) as a function of spin was also interpreted using the calculations based on the semiclassical particle-plus-rotor model (SCM) devised for shears bands [28–30]. Within the semiclassical framework of description of the

shears mechanism, the $B(M1)$ rate is given by [30]

$$B(M1) = \frac{3}{8\pi} j_\pi^2 g_{\text{eff}}^2 \sin^2\theta_\pi. \qquad (3)$$

θ_π is related to the shears angle θ, as [30]

$$\tan\theta_\pi = \frac{j_\nu \sin\theta}{j_\pi + j_\nu \cos\theta}. \qquad (4)$$

θ can be obtained from the relation,

$$\cos\theta = \frac{I_{sh}(I_{sh}+1) - [j_\nu(j_\nu+1) + j_\pi(j_\pi+1)]}{2[j_\nu(j_\nu+1) + j_\pi(j_\pi+1)]^{1/2}}. \qquad (5)$$

With the gradual closing of the neutron and proton angular momentum vectors, $\vec{j}_\nu$ and $\vec{j}_\pi$, the magnitude of $\vec{I}_{sh}$ ($= \vec{j}_\nu + \vec{j}_\pi$) increases along with a decrease in the $B(M1)$ values. The excitation energy of each state, however, would also be partly from the weakly deformed core as well as the closing of the shears. Thus, the observed spin, $I = I_{sh} + R_{\text{core}}$. A method of estimating the core contribution to the angular momentum for a shears band was discussed in Ref. [31]. The component from the weakly deformed core was assumed to be a linear function of angular momentum, i.e., $R_{\text{core}} = (\Delta R / \Delta I)(I - I_b)$ [27]. Here, I_b is the bandhead spin and $\Delta R / \Delta I = 0.36$ (for the present case).

The SCM calculations have been carried out for the 5qp-1 configuration, with $\vec{j}_\nu = 23/2$, $\vec{j}_\pi = 8$ and $g_{\text{eff}} = 0.9$. The calculated $B(M1)$ values show a decreasing trend as a function of spin which agrees with the experimental results (shown in Fig. 8). Hence, both the semiclassical and TAC calculations reasonably interpret the observed decreasing trend of the measured $B(M1)$ values with increasing spin, further confirming the MR nature of the 5qp-1 band.

The ^{107}Cd nucleus also has a pair of positive parity AMR bands [12], based on the 5qp neutron-proton configuration, $\pi(g_{9/2}^{-2}) \otimes \nu(h_{11/2}^2 g_{7/2})$. The newly explored MR band was found to be generated from the 5qp configuration, $\pi(g_{9/2}^{-2}) \otimes \nu(h_{11/2} g_{7/2}^2)$, which is further crossed by another 5qp configuration, $\pi(g_{9/2}^{-2}) \otimes \nu(h_{11/2}^3)$. Hence, both the MR and AMR bands observed in this nucleus are built on the 5qp neutron-proton configuration with different neutron configurations.

An interesting fact to be noticed about the nucleus is that, with the same number of unpaired neutrons and protons playing an active role, occupancy of an odd number of unpaired neutrons in the negative parity $h_{11/2}$ orbital, causes the two high-Ω $g_{9/2}$ proton hole angular momentum vectors to align towards each other with their resultant ($\vec{j}_\pi$) having a finite projection on the symmetry axis. The $\vec{j}_\pi$, and the resultant neutron angular momentum vector $\vec{j}_\nu$, form the two blades of a shear, with their resultant total spin, $\vec{I}_{sh}$ ($= \vec{j}_\pi + \vec{j}_\nu$), in between them (tilted axis cranking). The gradual closing of both the neutron and proton blades towards $\vec{I}_{sh}$ generates the high-spin states characterized by $M1$ transitions with decreasing $B(M1)$ values. On the other hand, with an even number of unpaired

neutrons in the low-Ω $h_{11/2}$ orbitals, the two high-Ω $g_{9/2}$ proton hole vectors stretch apart and become antialigned (no net projection on the symmetry axis), with the resultant neutron vector in between them and nearly perpendicular to each other, forming two shears of twin nature with the total angular momentum vector along $\vec{j}_\nu$. The gradual closing of the proton blades towards $\vec{j}_\nu$ generates the high-spin states characterized by $E2$ transitions with decreasing $B(E2)$ values.

To sum up, ^{107}Cd develops an MR band with the switching of one neutron from the $h_{11/2}$ in the AMR band to $g_{7/2}$. Hence, we see that the neutron occupancy plays the most important role in the coexistence of MR and AMR phenomena and a single particle can change the whole mechanism of generating the angular momentum.

V. SUMMARY

Negative parity $M1$ band structures have been discovered extending up to spin $49/2^{(-)}$ and decaying to the low-spin states ($19/2^-$ at 2159 keV and $23/2^-$ at 3115 keV) via several different paths. Lifetimes of the levels in the band up to spin $41/2^-$ have been measured using DSAM. The deduced $B(M1)$ values exhibit the characteristic decrease as a function of spin up to $39/2^-$, as expected for the shears mechanism.

The observed properties of the band before and after the backbend have been interpreted on the basis of TAC calculations for the configurations $\pi(g_{9/2}^{-2}) \otimes \nu(h_{11/2} g_{7/2}^2)$ (5qp-1) and $\pi(g_{9/2}^{-2}) \otimes \nu(h_{11/2}^3)$ (5qp-2), respectively. The calculated $B(M1)$ values for the 5qp-1 configuration agrees well with the experimentally obtained values, decreasing with increase in spin, a characteristic feature of an MR band. The calculated $B(M1)$ values for the 5qp-2 configuration are much smaller, but decrease with increasing spin, again a characteristic property of the MR band. Other than TAC calculations, the observed decreasing trend of the $B(M1)$ values is also reasonably supported by the semiclassical calculations for the 5qp-1 configuration.

Comparison of the experimental observations with the theoretical calculations ensures that the dipole band arises from magnetic rotation or shears mechanism, first arising from the 5qp-1 configuration which is then crossed by a second 5qp configuration (5qp-2). In addition, we find that ^{107}Cd is an example of an odd-A nucleus having coexistence of both the MR and AMR bands, both developed from 5qp configurations with same proton configuration, but different neutron configurations.

[1] S. Frauendorf, Spontaneous symmetry breaking in rotating nuclei, Rev. Mod. Phys. **73**, 463 (2001).

[2] Amita, A. K. Jain, and B. Singh, Table of magnetic dipole rotational bands, Atomic Data and Nuclear Data Tables **74**, 283 (2000); revised edition at http://www.nndc.bnl.gov/publications/preprints/mag-dip-rot-bands.pdf.

[3] A. K. Jain and D. Choudhury, Magnetic rotation – past, present and future, Pramana-Journal of Physics **75**, 51 (2010).

[4] S. Frauendorf, Tilted cranking, Nucl. Phys. A **557**, 259 (1993).

[5] D. Choudhury et al., Evidence of antimagnetic rotation in odd-A ^{105}Cd, Phys. Rev. C **82**, 061308(R) (2010).

[6] R. M. Clark et al., The shears mechanism in the lead isotopes, Phys. Lett. B **440**, 251 (1998).

[7] N. S. Kelsall et al., Evidence for shears bands in ^{108}Cd, Phys. Rev. C **61**, 011301(R) (1999).

[8] S. Roy et al., Band crossing in a shears band of ^{108}Cd, Phys. Rev. C **81**, 054311 (2010).

[9] A. J. Simons et al., Investigation of antimagnetic rotation in light Cadmium nuclei: ^{106,108}Cd, Phys. Rev. C **72**, 024318 (2005).

[10] P. Datta et al., Observation of antimagnetic rotation in ^{108}Cd, Phys. Rev. C **71**, 041305 (2005).

[11] D. Jerrestam, F. Lidén, J. Gizon, L. Hildingsson, W. Klamra, R. Wyss, D. Barnéod, J. Kownacki, Th. Lindblad, and J. Nyberg, Rotational bands in ^{107}Cd, Nucl. Phys. A **545**, 835 (1992).

[12] D. Choudhury et al., Multiple antimagnetic rotation bands in odd- A ^{107}Cd, Phys. Rev. C **87**, 034304 (2013).

[13] R. Palit et al., A high speed digital data acquisition system for the Indian National Gamma Array at Tata Institute of Fundamental Research, Nucl. Instrum. and Meth. in Phys. Research A **680**, 90 (2012).

[14] H. Tan et al., Digital data acquisition modules for instrumenting large segmented germanium detector arrays, in *Proceedings of the IEEE Nuclear Science Symposium Conference Record NSS 08* (IEEE, Washington, DC, 2008), p. 3196.

[15] Computer code DAMM: MILNER PACKAGE, the Oak Ridge analysis software (private communication).

[16] D. C. Radford, ESCL8R and LEVIT8R: Software for interactive graphical analysis of HPGe coincidence data sets, Nucl. Instrum. Methods A **361**, 297 (1995).

[17] J. C. Wells and N. R. Johnson, "LINESHAPE": A computer program for Doppler-broadened lineshape lifetime analysis, ORNL Physics Division Progress, Report No. ORNL-6689, September 30 (1991).

[18] A. Krämer-Flecken, T. Morek, R. M. Lieder, W. Gast, G. Hebbinghaus, H. M. Jäger, and W. Urban, Use of DCO ratios for spin determination in γ-γ coincidence measurements, Nucl. Instrum. Methods A **275**, 333 (1989).

[19] K. Starosta et al., Experimental test of the polarization direction correlation method (PDCO), Nucl. Instrum. Methods A **423**, 16 (1999).

[20] L. C. Northcliffe and R. F. Schilling, Range and stopping-power tables for heavy ions, Atomic Data and Nucl. Data Tables **7**, 233 (1970).

[21] F. James and M. Roos, Minuit - a system for function minimization and analysis of the parameter errors and correlations, Comput. Phys. Commun. **10**, 343 (1975).

[22] U. Hagemann, H. F. Brinckmann, W. D. Fromm, C. Heiser, and H. Rotter, Observation of isomeric states and band structures in ^{107}Cd, Nucl. Phys. A **228**, 112 (1974).

[23] V. I. Dimitrov, F. Dönau, and S. G. Frauendorf, Hybrid version of the tilted axis cranking model and its application to ^{128}Ba, Phys. Rev. C **62**, 024315 (2000).

[24] Amita, A. K. Jain, V. I. Dimitrov, and S. G. Frauendorf, Magnetic dipole rotational bands in odd-A Rb isotopes, Phys. Rev. C **64**, 034308 (2001).

[25] P. Agarwal et al., Bandcrossing of magnetic rotation bands in ^{137}Pr, Phys. Rev. C **76**, 024321 (2007).

[26] G. Andersson et al., Nuclear shell structure at very high angular momentum, Nucl. Phys. A **268**, 205 (1976).

[27] C. J. Chiara et al., Shears mechanism in ^{109}Cd, Phys. Rev. C **61**, 034318 (2000).

[28] A. O. Macchiavelli, R. M. Clark, P. Fallon, M. A. Deleplanque, R. M. Diamond, R. Krücken, I. Y. Lee, F. S. Stephens, S. Asztalos, and K. Vetter, Semiclassical description of the shears mechanism and the role of effective interactions, Phys. Rev. C **57**, R1073 (1998); A. O. Macchiavelli, R. M. Clark, M. A. Deleplanque, R. M. Diamond, P. Fallon, I. Y. Lee, F. S. Stephens, and K. Vetter, Rotational-like properties of the shears bands, *ibid.* **58**, 3746 (1998).

[29] R. M. Clark et al., Shears Mechanism in the A ∼ 110 region, Phys. Rev. Lett. **82**, 3220 (1999).

[30] R. M. Clark and A. O. Macchiavelli, The shears mechanism in nuclei, Annu. Rev. Nucl. Part. Sci. **50**, 1 (2000).

[31] A. O. Macchiavelli, R. M. Clark, M. A. Delephanque, R. M. Diamond, P. Fallon, I. Y. Lee, F. S. Stephens, and K. Vetter, Shears mechanism and particle-vibration coupling, Phys. Rev. C **58**, R621 (1998).